

## INSTRUMENTATION

## A Comparison of Count Rate Parameters in Gamma Cameras

Thomas K. Lewellen and Robert Murano

*University of Washington, Seattle, Washington*

**Pulse pile-up is a fundamental problem that limits the ability of a gamma camera to produce high quality images at high count rates. Pulse pile-up results in loss of events and spatial distortions in the image. The question asked in this study is how well do some of the test procedures for measuring count rate performance in gamma cameras compare. In four gamma cameras we compared measurements of spectral fraction, count-rate curve, pulse-pair resolution, deadtime, maximum count rate, full width at half maximum of the line spread function, and misplaced event count rate. The results indicated that no one technique provides a complete description of the count-rate effects in gamma cameras. The misplaced-event measurements provided the most information.**

**J Nucl Med 22: 161-168, 1981**

The basic problem that limits the ability of most modern gamma cameras to produce good images at high count rates (count-rate performance) involves pulse pile-up in the NaI(Tl) detector (1) and in the pulse-shaping amplifiers (1-3). Since the NaI(Tl) detector places inherent limitations on count-rate performance (1), camera designers have paid great attention to amplifier design and the inclusion of pile-up rejection circuits in pulse-height analyzers (PHA). The amplifier systems have a characteristic shaping time or period, during which the detector pulse is integrated. In such a system, a compromise is made between obtaining optimal energy resolution (long shaping times) and high count-rate performance (short shaping times).

The pulse-shape time constant is directly related to the parameter termed the pulse-pair resolution, which is the longest interval between two incoming pulses that will result in a single output pulse from the amplifier. When two pulses are separated in time by a period less than or equal to the pulse-pair resolution, the system will lose an event (this is essentially the concept of deadtime). The higher the count rate, the greater the percentage of events that will be lost.

The effects of pile-up in an imaging system are more severe than loss of counts. The pulse produced from two fused events "looks" like a single event with an energy approximately equal to the sum of the two events, and will be assigned a position that is generally somewhere between the actual positions of the two original events. Thus, not only are events lost, but position information is distorted. In general, if a piled-up pulse can be discriminated against, either by energy discrimination or special pile-up rejection circuits (2,3), image quality will be improved.

There are many possible results when two pulses pile-up. If two events that should be accepted pile up, the resulting pulse will generally be rejected by the camera PHA. The result is a loss of two valid events, but the rejection prevents the recording of a misplaced event. If a low-energy pulse and a "valid" pulse pile up and the resulting pulse is rejected by the PHA, a valid event is lost, but again a misplaced event is not recorded. If a low-energy pulse and a valid event pile up and are accepted by the PHA, the valid event is accepted, but its indicated position will be wrong. If two low-energy pulses pile up and are accepted by the PHA, an invalid event will be recorded.

The study reported here examines the question of how well several of the more common tests used to characterize count-rate performance compare, particularly in view of the problems of count loss and misplaced events.

Received June 5, 1980; revision accepted Aug. 29, 1980.

For reprints contact: Thomas K. Lewellen, PhD, Div. of Nuclear Medicine, University Hospital, Univ. of Washington, Seattle, WA 98195.

The parameters compared were spectral fraction, deadtime (the Adams technique, Ref. 4), full field count-rate curve, full width at half maximum (FWHM) of the line spread function, pulse-pair resolution, and misplaced events.

#### METHODS

**Spectral fraction.** The spectral fraction is the percentage of the total detected events that were within the gamma camera's PHA window. A lead ring was placed on the detector (collimator removed) to mask the system to the useful field of view. A multichannel analyzer (MCA) was interfaced to the total energy signal from the camera. A small Tc-99m point source was placed 1.8 m above the detector. Using a symmetric 15% PHA window, the camera was peaked for 140 keV at a count rate less than 5,000 cps. A series of calibrated lead apertures in front of the point source is used to vary the detector count rate, and the spectral fraction was measured with the MCA. The total detector count rate for each measurement was based on the low-count-rate data. First, the total detector rate for the lowest observed count rate was calculated using the spectral fraction as measured with the MCA (total = observed/fraction). Then the total rate for the other measurements was calculated using previously determined calibrations for the various apertures (total expected = total in first measurement  $\times$  aperture calibrations  $\times$  half life corrections). The apertures used were 3-mm thick, 30-mm diameter lead disks with holes drilled through the center. Calibration factors for each disk for use with the spectral fraction and count-rate curve measurements were determined using a series of sources at different activities. The source strength was measured with a dose calibrator, and each source disk combination was selected to keep the count rate through a 20% window on a 380-mm field of view camera below 5,000 cps. The count rate through each aperture and the spectral fraction for each aperture were measured with background corrections using both a 340 and 254-mm field of view camera. The values were then normalized to the same source strength, and the spectral fraction was used to generate a table of percentage transmission as a function of aperture hole size and PHA window width.

**Deadtime.** The procedure for deadtime measurement used was developed by R. Adams, et al. (4). The technique assumes a paralyzable deadtime model with no correction for spectral fraction and uses scattering conditions similar to those in clinical cardiac studies. The cameras were first peaked with Tc-99m with a symmetric 20% window and no scattering material. Two Tc-99m sources in 12-cm long tubes were prepared, each source producing approximately 20,000 cps when placed in the phantom. The count rates for source one ( $R_1$ ), sources one and two ( $R_{12}$ ), and source two ( $R_2$ ) in the

phantom were determined. The paralyzable "deadtime" was calculated from:

$$t \text{ (}\mu\text{sec)} = 10^6 \times \frac{2R_{12}}{(R_1 + R_2)^2} \ln \frac{(R_1 + R_2)}{R_{12}}$$

**Count-rate curve.** This procedure was used to determine expected count rate from the observed under intrinsic flood-field conditions (no scatter), as well as the pulse-pair resolution and maximum count rate. A lead ring was placed on the detector (collimator removed) to restrict the system to the useful field of view. A multichannel analyzer (MCA) was interfaced to the total signal from the camera (5). The camera was peaked for Tc-99m using a symmetric 15% window and a small source 1.8 m above the detector. Using calibrated apertures in front of the source holder, the expected count rate was determined by combining the aperture calibrations and the low-count-rate spectral fraction (i.e., under conditions of no observable pile-up effects) to determine the total detector count rate for the small aperture. Then the aperture calibrations and spectral fractions were used to calculate the expected count rate for the larger apertures. Thus the expected count-rate calculation assumed there would be no pulse pile-up. The pulse-pair resolution was determined by fitting the low-count rate data to the equation  $R_0 = DF \exp(-TD)$ , where  $R_0$  was the observed count rate,  $D$  was the total detector count rate,  $F$  was the spectral fraction, and  $T$  was the pulse pair resolution (6). The maximum count rate was determined by inspection of the data plots.

**Line spread function.** Measurement of the FWHM of the intrinsic line spread function was used as an indicator of spatial distortion against count rate. A lead plate with several parallel slots 0.5 mm wide on 30 mm centers was placed on the detector (collimator removed) with the slots perpendicular to the detector x axis. Additional lead plates were used to mask the slots such that only a 1-cm length of each slot is exposed. A 1-cm long line will affect the accuracy of the LSF measurement to a small extent due to the long tails of a detector's response to points of activity. Since the measurement was of relative changes in FWHM value, however, the absolute value of FWHM was not of concern.

A small Tc-99m point source was placed above the detector and a symmetric 15% PHA window was set. The count rate was increased by moving the source closer to the plate. The FWHM was measured for several line segments at each counting rate, and the results corrected for the effects of slot width as determined with weaker sources at the same distance from the plate.

The correction was made by subtracting the FWHM of the LSF for the weak source (camera count rate < 5,000 cps) from the LSF for the strong source at each distance. The subtraction was done by taking the square root of the difference of the squares of the FWHM values.

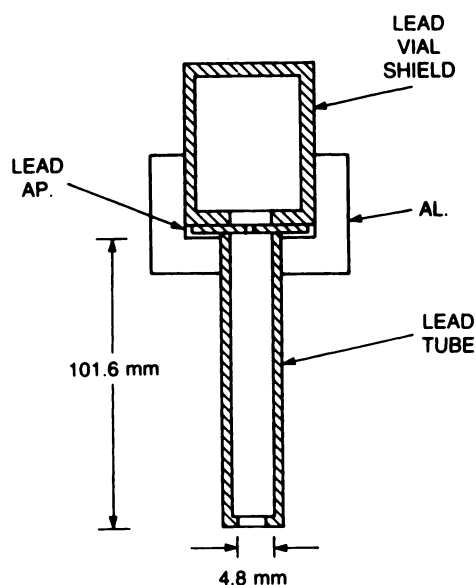


FIG. 1. Diagram of lead shield and collimator system used to hold "point" sources for misplaced-events measurements. A 3-cc vial with 40 mCi of Tc-99m was placed inside lead shield. Shield is removable to allow changing to plates.

**Misplaced events.** A measurement was made of the occurrence of misplaced events and total observed count rate against expected count rate. The technique differs from previously published methods (2,3) in that collimated point sources were used to illuminate the detector with collimator absent. The sources consisted of a 3-cc lead vial shield with a hole bored in the bottom, a lead tube, and a set of apertures (Fig. 1).

The apertures were calibrated in a manner similar to that used for the spectral fraction and full field count-rate curve data. For the small source-holder calibrations, a 229-mm diameter, 10-cm thick NaI(Tl) detector was used. Each holder-aperture pair was calibrated as a unit with a series of sources. The source strengths, measured in a dose calibrator, were selected to keep the detector count rate through a 20% window less than 3,000 cps for each aperture. Each aperture was measured ten times

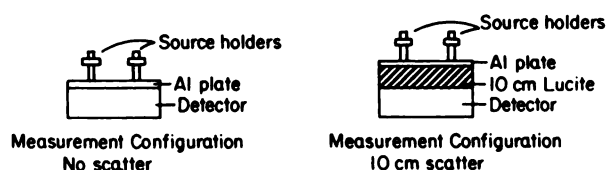


FIG. 2. Diagram of placement of source holder for misplaced-events measurements. Aluminum plate has holes on 25.4 mm centers, which are used to position source holders.

with a new set of sources for each measurement. The final calibration was the average of the ten measurements.

For the camera measurements, a 3-cc vial containing 40 mCi of Tc-99m was placed in each source holder. The source holders were positioned on the detector (collimator removed) with the aid of an aluminum plate with a series of holes bored in it (Fig. 2). The count rate was altered by using the apertures. The expected count rate was determined using spectral fraction data (taken concurrently), aperture calibrations and the total observed events at observed count rates below 5,000 cps. The expected count rate was then calculated for each aperture using the previously determined calibration data and making the assumption that there will be no pile-up effects (expected cps = [total with smallest aperture]  $\times$  spectral fraction  $\times$  aperture calibration).

The data were acquired on a clinical computer system. The images were processed in a manner similar to that reported by Murphy (2). The lowest count-rate data were used to determine the point spread functions (PSF) for the sources. The resulting PSFs were then subtracted from the frames for the higher count-rate data, and the remainder summed as misplaced events. A major concern of the technique was the effect of the different aperture sizes on the PSF shape. The PSF for each aperture, using count rates less than 5,000 cps, was determined and the results compared. The area under the PSF differed by less than 1% between the apertures. Since the percentage of misplaced events measured was generally much greater than 1%, the geometrical effect on the

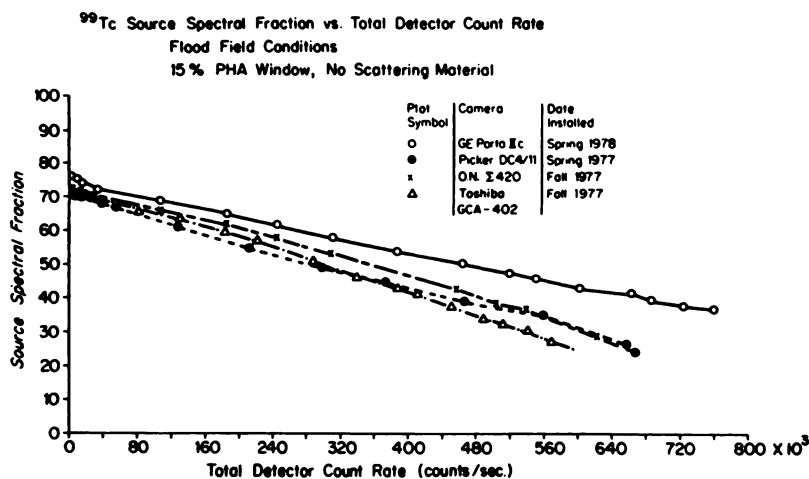
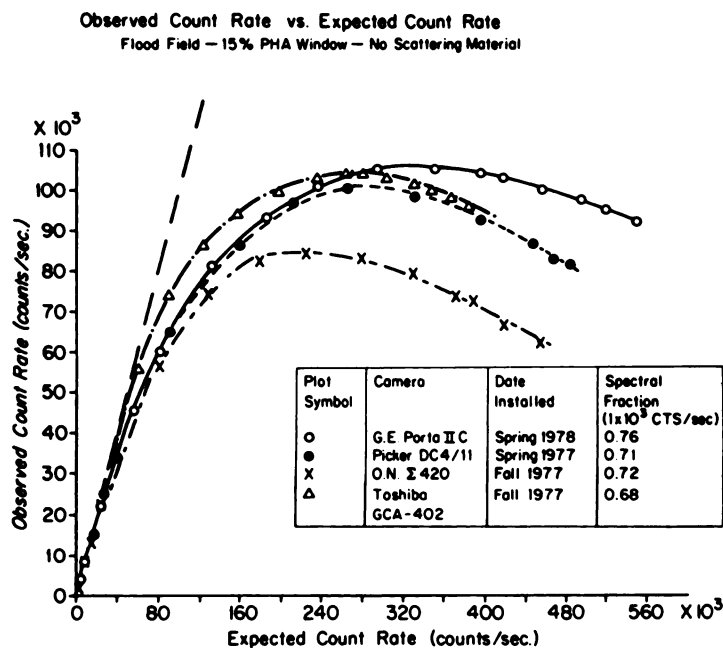


FIG. 3. Spectral fraction data for four cameras are plotted versus ideal total detector count rate—i.e., count rate if there were no pile-up. See text for procedure.



**FIG. 4.** Observed count rate versus expected count rate for four cameras. Small Tc-99m source was positioned 1.8 m above detector (no collimator). Dashed line is expected result for a system with no deadtime or pile-up. See text for estimation of expected count rate.

PSFs was neglected in analyzing the misplaced events data.

#### RESULTS

Data were acquired from four cameras: A General Electric Porta IIC installed in the spring of 1978, a Picker DC4/11 installed in the spring of 1977, an Ohio Nuclear Sigma 420 installed in the fall of 1977, and a Toshiba GCA 402 installed in the fall of 1977. The instruments were in routine clinical use and were not subjected to any special service inspections before the tests. These cameras should not be regarded as typical examples of the equipment produced by any manufacturer. The data presented here are to demonstrate the different results that can be obtained with the different measurement techniques being compared.

The spectral-fraction data are shown in Fig. 3. The fraction measured for each camera is plotted against the total detector count rate. The 15% window settings were selected from the standard range of choices on the control consoles and were not checked for accuracy. Plots of the observed count rate against the expected count rate for the same set of instruments are shown in Fig. 4. The dashed line indicates the ideal response (i.e., no count loss). The maximum count rate and pulse-pair resolution as determined from the data in Fig. 4 are listed in Table 1. Table 1 also lists the results of the deadtime measurements. A comparison of the pulse-pair and deadtime values indicates some differences in the cameras. Figure 5 plots the line spread against cps and indicates differences between the cameras measured. Figures 6, 7, and 8 show the incidence of misplaced events. In each figure the dashed line indicates the performance for a "perfect" system. In Fig. 6 two sets of

data are shown: the total observed events and the misplaced events with no scattering material. Figure 7 shows the same data except that scattering material (10 cm of Plexiglas) is placed between the sources and the detectors. Figure 8 plots the percentage of the total observed count attributed to misplaced events against the expected count rate for the no-scatter case.

#### DISCUSSION

The measurements of spectral fraction do not indicate the effectiveness of pile-up rejection circuits, which operate after the pulse-shaping amplifiers. There are differences in the shapes of the curves in Fig. 3 as count rate increased (compare G.E. and Picker with O.N. and Toshiba). These differences may reflect basic design

**TABLE 1. DEADTIME, PULSE PAIR, AND MAXIMUM COUNT RATE DATA**

Camera	Deadtime (μsec)	Pulse pair (μsec)	Maximum cps
G.E. Porta IIC Installed Spring 1978	4.7	1.7	106,000
Picker DC4/11 Installed Spring 1977	4.8	1.7	101,000
O.N. Sigma 420 Installed Fall 1977	6.7	2.0	85,000
Toshiba GCA-402 Installed Fall 1977	7.2	1.5	105,000

Intrinsic Line Spread Function vs. Observed Count Rate  
15% PHA window

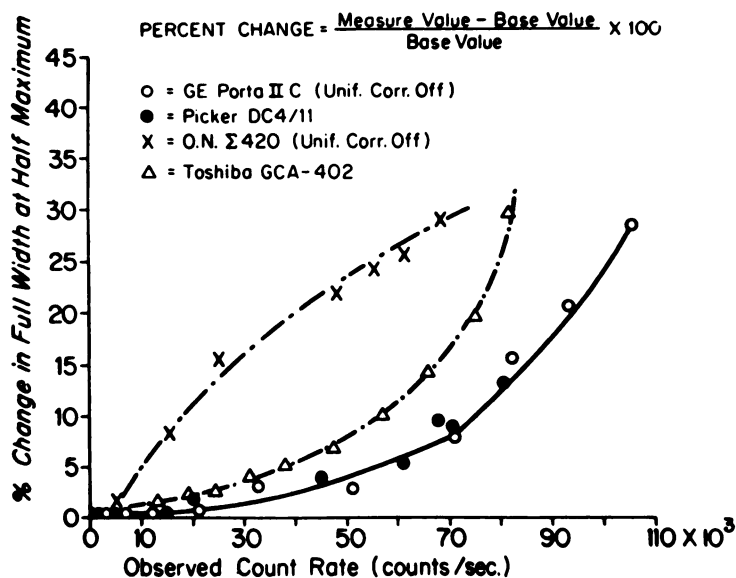


FIG. 5. Intrinsic line spread functions versus observed count rate for cameras. Small Tc-99m source is masked by lead sheet containing slots 0.5 mm wide by (in effect) 1 cm long. Count rate is varied by moving source closer to slot, requiring geometrical corrections for data.

information of importance in understanding subtle differences in system performance, but they are not immediately translatable into clinically meaningful terms.

The data in Table 1 do indicate some differences among the cameras studied. The values for maximum count rate are less than those normally published by the manufacturers, due to the window width used in the study. Larger windows increase the maximum count rate

but also accept more piled-up (false) pulses. In this instance, the maximum count rates for G.E., Picker, and Toshiba are essentially the same, whereas the Ohio Nuclear system is lower. The pulse-pair resolutions are all essentially the same. This is to be expected since three cameras use approximately the same time constants in the shaping amplifiers.

The deadtime values also show differences between the cameras. Measurements of deadtime are highly de-

Total Observed and Misplaced Event Count Rate  
Versus Expected Count Rate

TWO SOURCES - NO SCATTER - 15% PHA WINDOW

Plot Symbol	Camera	Date Installed	Spectral Fraction
o	GE Porta II C	Spring 1978	0.74
●	Picker DC4/11	Spring 1977	0.69
x	O.N. Σ420	Fall 1977	0.70
Δ	Toshiba GCA-402	Fall 1977	0.68

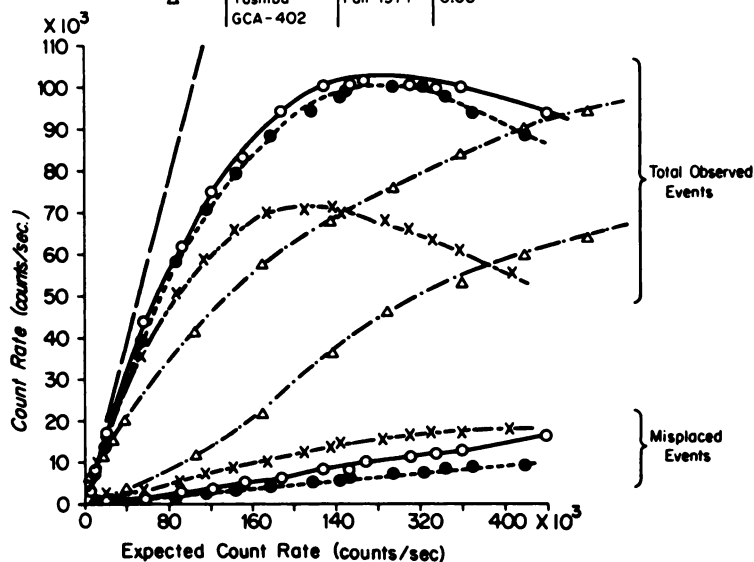


FIG. 6. Total observed and misplaced count rates versus expected count rates for cameras studied. Conditions provide no scatter. Dashed line indicates total observed count rate for system with no deadtime or pile-up. See text for procedure.

## Total Observed and Misplaced Events vs. Expected Count Rate

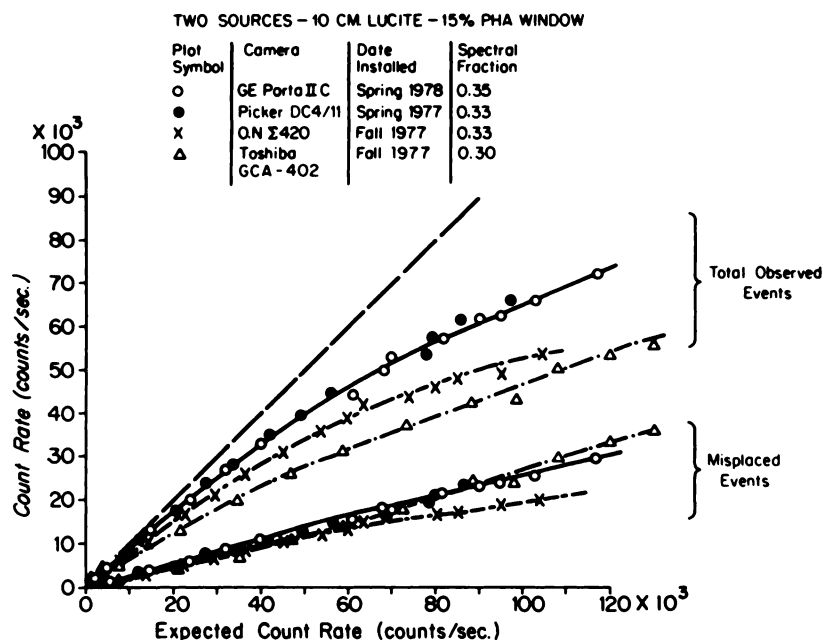


FIG. 7. Total observed and misplaced count rates versus expected count rates for cameras studied. Conditions include 10 cm of scattering material. Dashed line indicates total observed count rate for system with no deadtime or pile-up. Procedures as in Fig. 6, see text.

pendent on window width, photopeak centering, and scatter conditions (6-8). In this case, considerable care was taken to use the same measurement conditions for all cameras. Thus, the smaller deadtime values for the G.E. and Picker systems in comparison to the other camera systems are reproducible. The count-rate curves of Fig. 4 also demonstrate differences between the cameras. In comparing the deadtime measurement results with the curves of Fig. 4 and the pulse-pair observations, we apparently find major discrepancies. In particular, note the differences between the results for the Toshiba camera. The count-rate curve (measured with no scattering material) suggests that the Toshiba would lose the least counts, whereas the deadtime values (measured with scattering material) indicate the Toshiba would lose the most counts. This apparent inconsistency illustrates the important point that the count-rate performance of a gamma camera is dependent on the source geometry and the amount of scattering material present.

The line-spread data (Fig. 5) are not precise since they had to be corrected for large geometrical effects when the source was brought close to the plate in order to produce the higher count rates. The corrections for the highest count rates were on the order of 50%. The results do indicate that for the cameras tested there are some major differences. Presumably, the increase in width of the FWHM reflects spatial distortions caused by pile-up. Such distortions are most likely to be due to misplaced events and, as expected, the misplaced-event data of Figs. 6, 7, and 8 demonstrate differences between the cameras.

The data of Fig. 6 characterize both event loss (total observed count rate) and pile-up effects causing pulse

distortion (misplaced events). The use of two small sources represents a greater concentration of activity per unit area than is normally found in vivo and in that sense is nonclinical. The two measurement conditions (no scatter, and 10 cm of Plexiglas with no camera collimator) represent extremes of performance, with actual clinical conditions falling somewhere in between these. The scatter conditions used for the data in Fig. 7 are much worse than those found clinically, since the detector is uncollimated. The data show major differences between the cameras in the nonscatter conditions, although the differences become less severe under scatter conditions used in this study. The differences between cameras in more clinically relevant scatter conditions should be greater than indicated by Fig. 7, as has been demonstrated by Strand et al. (1,3). The performance of each camera is degraded significantly by scatter, as is expected due to the much higher total detector count rate for the corresponding expected rate from the PHA window, and the increased chance of pile-up due to the large number of low-energy events.

The representation of the data as percent misplaced events (Fig. 8) is interesting but does not convey the event-loss information of the curves for total observed rate and misplaced-event rate. One should compare these data with the "total count rate" curves of Fig. 4 and the deadtime measurements. The lower maximum count rate values observed in Fig. 6 are most likely due to the many lead x-rays present in the misplaced-event measurements used in this study. The lead shields produce a large flux of x-rays, which interact in the detector, reducing the spectral fraction. Thus, the observed count rate in the misplaced events corresponds to a higher detector count rate than is produced in the count rate

# Percent Misplaced Events vs. Expected Count Rate

Two Sources — No Scatter — 15 % PHA Window

Plot Symbol	Camera	Date Installed	Spectral Fraction
○	G.E. Porta II C	Spring 1978	0.74
●	Pickar DC4/11	Spring 1977	0.69
x	O.N. Σ420	Fall 1977	0.70
Δ	Toshiba GCA-402	Fall 1977	0.68

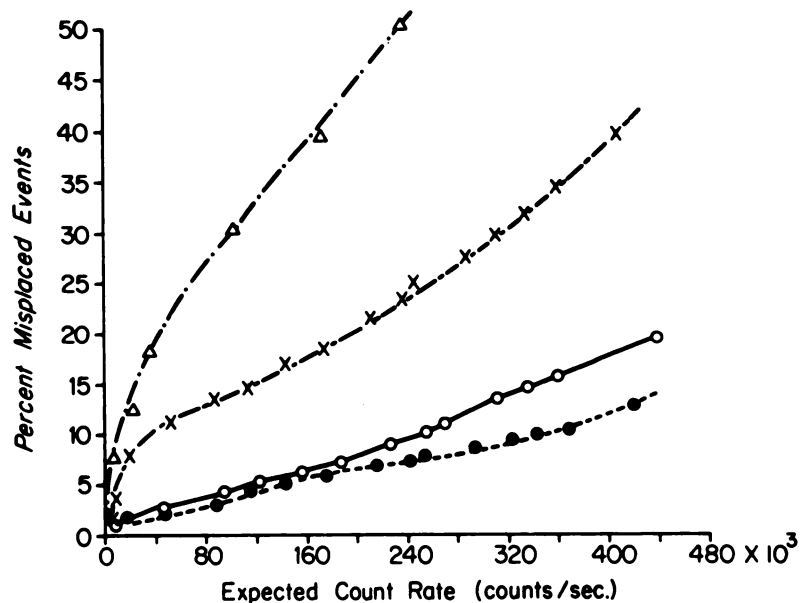


**FIG. 8.** Percent misplaced events versus expected count rate for cameras studied. No-scatter conditions. Dashed line indicates the total observed count rate for system with no deadtime or pile-up. See text for procedure.

curves of Fig. 4. Since loss of counts is primarily a function of the total detector count rate (6), the maximum count rate will be lower in the misplaced event technique.

Our misplaced-event technique was selected due to the long data acquisition times of the decaying-source techniques (2,3). This study used 20 apertures in each source holder to vary the counting rates. If a set of sources were to be used, 40 TC-99m sources would have to be made and calibrated for each data run, a rather difficult task. The aperture method does allow the data to be acquired rapidly, but the analysis is much more difficult, especially due to the large flux of lead x-rays generated in the shield.

## CONCLUSIONS

We draw several conclusions from the findings of this study. First, no one measurement adequately describes the count-rate performance of a gamma camera. Second, the misplaced-event measurements provide the most information, characterizing event loss as well as event distortion. Third, if misplaced measurements cannot be performed, the deadtime measurement (characterizing event loss under conditions similar to those of clinical imaging) is the next most useful measurement. In reviewing the data, it is important to remember that all the

results are technique-dependent. The absolute values can change significantly if the measurement conditions are altered.

The comparisons show that if only one parameter were measured, severely restricted conclusions about the performance of a system could be made. For example, compare the results of the count-rate curve (Fig. 4), misplaced events (Fig. 6), and deadtime (Table 1). Clearly, camera performance is dependent on the source distribution and the presence of scatter. Most of the techniques cover a range of counting rates much greater than those encountered in most clinical situations. In such measurements, the data in the clinical range of counting rates (20,000–40,000 observed cps in most cases) should be the primary area of interest.

The frequency of misplaced events, although relatively small for most clinical counting rates, is an important parameter, since the pulse distortion represented by misplaced events degrades low-contrast resolution. Techniques to characterize low-contrast performance with less sophisticated equipment would be of particular value in assessing the count-rate performance of gamma cameras.

## REFERENCES

1. STRAND S-E, LAMM I-L: Theoretical studies of image arti-

- facts and counting losses for different photon fluence rates and pulse-height distributions in single-crystal NaI(Tl) scintillation cameras. *J Nucl Med* 21: 264-275, 1980
2. MURPHY P, ARSENEAU R, MAXON E, et al: Clinical significance of scintillation camera electronics capable of high processing rates. *J Nucl Med* 18: 175-179, 1977
  3. STRAND S-E, LARSSON I: Image artifacts at high photon fluence rates in single-crystal NaI(Tl) scintillation cameras. *J Nucl Med* 19: 407-413, 1978
  4. ADAMS R, HINE GJ, ZIMMERMAN CD: Deadtime measurements in scintillation cameras under scatter conditions simulating quantitative nuclear cardiology. *J Nucl Med* 19: 538-544, 1978
  5. LEWELLEN TK, WILLIAMS DL, MURANO RM, et al: A field procedure for the quantitative assessment of nuclear imaging cameras. *J Nucl Med* 19: 954-958, 1978
  6. ARNOLD JE, JOHNSTON AS, PINSKY SM: The influence of true counting rate and the photopeak fraction of detected events in Anger camera deadtime. *J Nucl Med* 15: 412-416, 1974
  7. SORENSON JA: Methods of correcting Anger camera deadtime losses. *J Nucl Med* 17: 137-141, 1976
  8. SORENSON JA: Deadtime characteristics of Anger cameras. *J Nucl Med* 16: 284-288, 1975

## ANNUAL SPRING MEETING Pacific Northwest Chapter Society of Nuclear Medicine

**March 27-29, 1981**

**Alderbrook Resort  
ANNOUNCEMENT**

**Union, Washington**

Drs. Raymond Marty, Program Chairman and Michael Graham, Program Co-Chairman announce the following plans for the Pacific Northwest Chapter Spring Meeting.

Clinical Aspects of single photon emission tomography.  
Practical aspects and applications of the 400T system.

John Keyes, M.D.  
Dave Williams, M.D., James  
Ritchie, M.D., James Cald-  
well, M.D., and Glen Hamil-  
ton, M.D.  
Thomas Davis, M.D.

Combined Imaging Modalities in the evaluation of the Abdomen.  
Nuclear Medicine, Ultrasound, CAT scans and conventional radiography in the  
evaluation of renal function.  
Evaluation of the gallbladder and biliary tree by various imaging modalities.  
General overview of the various imaging modalities and their appropriateness and  
cost effectiveness.

Tom Rudd, M.D.  
John Denney, M.D.

Wil Nelp, M.D.

There will also be a Technologist sponsored program.  
Application for AMA category I credit for physicians will be on file.  
There will be a Chapter General Business Meeting on Saturday, March 28, 1981 at the scheduled lunch.  
For further information and hotel and registration cards, please contact: Jean Parker, Administrator, Pacific Northwest  
Chapter, SNM, P.O. Box 40279, San Francisco, CA 94140.

## NUCLEAR CARDIOLOGY 1981

**March 21-25, 1981**

**Innisbrook**

**Tarpon Springs, Florida**

Waterbury Hospital Health Center in conjunction with Yale University School of Medicine will present a general review course in Nuclear Cardiology, March 21-25, 1981 at Innisbrook, Tarpon Springs, Florida. The course will include general techniques and clinical applications utilizing a format of lectures and workshop presentations. Registration is open to physicians in all fields of medicine interested in noninvasive cardiovascular diagnosis.

The Program Directors are Gerald R. Berg and Robert Toffler. Course Directors are Paul Hoffer, Barry L. Zaret, and Alexander Gottschalk. The faculty will also consist of H. William Strauss, Franz J. Th. Wackers, Harvey J. Berger, Lawrence S. Cohen, and Glenn Hamilton.

The fee is \$300 (\$150 for residents) and 19 hours of category I credit may be obtained.

For further information, contact: Gerald R. Berg, M.D., Department of Radiology, Waterbury Hospital Health Center, 64 Robbins St., Waterbury, CT 06720. Tel: (203) 573-7124.